The pH effect on the kinetics of 4-nitrophenol removal by CWPO with doped carbon black catalysts

Jose L. Diaz de Tuesta[a,b,*], Asuncion Quintanilla[c], Jose A. Casas[c], Sergio Morales-Torres[d], Joaquim L. Faria[b], Adrián M.T. Silva[b], Helder T. Gomes[a,b]

[a] Centro de Investigação de Montanha (CIMO), Instituto Politécnico de Bragança, Campus de Santa Apolónia, 5300-253 Bragança, Portugal
[b] Laboratory of Separation and Reaction Engineering - Laboratory of Catalysis and Materials (LSRE-LCM), Faculdade de Engenharia, Universidade do Porto, Rua Dr. Roberto Frias, 4200-465 Porto, Portugal
[c] Departamento de Ingeniería Química, Facultad de Ciencias, Universidad Autónoma de Madrid, Cantoblanco, Ctra. de Colmenar km 15, 28049 Madrid, Spain
[d] Carbon Materials Research Group, Department of Inorganic Chemistry, Faculty of Sciences, University of Granada, Campus Fuentenueva s/n, 18071 Granada, Spain

ARTICLE INFO

ABSTRACT

P, B and N-doped carbon blacks prepared with H_3PO_4, urea and H_3BO_3 were tested as catalysts in the wet peroxide oxidation of a concentrated 4-nitrophenol (4-NP) model solution ($C_{4-NP} = 5$ g·L^{-1}). The highest catalytic activity was found for P-doped carbon black (complete removal of 4-NP after 4 h at 80 °C, $C_{cat} = 2.5$ g·L^{-1}, $C_{H_2O_2} = 17.8$ g·L^{-1} and initial pH 3, whereas 44-19% removals were reached with the other catalysts). That was ascribed to the strongest acidity ($pH_{PZC} = 3.5$) and hydrophilic character of the catalyst. Initial pH affected the oxidation, allowing to increase strongly the conversion of 4-NP with the P-doped catalyst decreasing the initial pH from 4 to 2 (4-NP removal from 20% to 99% after 8 h of reaction time at 50 °C, $C_{cat} = 2.5$ g·L^{-1} and $C_{H_2O_2} = 17.8$ g·L^{-1}). An autocatalytic-power-law kinetic model was developed to predict the observed induction period and the dependence on the pH of the 4-NP oxidation, H_2O_2 consumption and pH evolution ($k_{4-NP} = 2.2 \cdot 10^{-5}$ M^{-2} min^{-1}, $k_{H_2O_2} = 4.0 \cdot 10^{-6}$ M^{-3}·min^{-1} and $k_{H^+} = 5.1 \cdot 10^{-3}$ M$^{-0.23}$ min^{-1} at 80 °C).

1. Introduction

The complexity of industrial wastewaters requires the development of more efficient and economically viable treatment technologies. In particular, nitrophenols (NPs), whether mono-, di- or tri-nitrophenols, are contaminants commonly present in wastewaters of plastic, pharmaceutical, paper, pesticide, synthetic dyes, insecticides, herbicides and explosive industries, reaching high concentrations in these effluents [1,2]. NPs are well-known to be highly toxic, inhibitory and bio-refractory organic compounds [3,4]. The degradation rate of NPs is quite slow in wastewater treatment plants, and moderate in soil, and both acute and chronic effects have been reported for animals and humans [4]. The United States Environmental Protection Agency (USEPA) included those NPs in the list of priority pollutants [5] and reported maximum allowable concentrations in water of 20 ppb [6].

Advanced oxidation processes (AOP) are particularly useful technologies to treat nondegradable compounds present in wastewaters in a wide range of initial concentrations (0.001–10 g·L^{-1}) [7–9], difficult to remove by the conventional biological processes [10–14]. In this context, different AOPs have been studied, such as ozonation [15,16], photo-degradation [17,18] and electrochemical oxidation [19,20]. All these techniques allow to remove completely 4-NP after 0.25–6 h depending on conditions tested. The main drawback of these processes is the expensive reagent and energy source necessities. Trapido and Kallas evaluated the degradation of 4-NP by different AOPs, such as Fenton, ozonation and photo-degradation, concluding that the Fenton reagent was found to be the most promising for the abatement of 4-NP [21]. Thenceforward, the removal of 4-nitrophenol (4-NP) by oxidation with hydrogen peroxide (H_2O_2) has been studied applying Fenton and intensified Fenton treatments, such as photo-Fenton [3,22–24], microwave-assisted Fenton [25] and electro-Fenton [26–28] processes. The non-intensified Fenton process is able to totally remove 4-NP after 2 h (considering 1 mM of 4-NP at 25 °C, pH = 3, > 5 mM of H_2O_2 and > 5 mg/L of Fe^{2+}) [29]. However, the Fenton process requires the recovery of the Fe catalyst at the end of treatment and a rigorous pH control to efficiently run the process. Within this context, catalytic wet peroxide oxidation (CWPO) appears more advantageous AOP [30,31], since run with a heterogeneous catalyst which can be recovered after

the process [11,32,33]. However, most of the studies regarding the CWPO of 4-NP deals with the development of catalysts containing iron, such as hybrid magnetic graphitic nanocomposites [34], nano-magnetite [35], fly ash [36], ferrous hydroxide colloids [37], Fe/Cu/Zr-clays [38], or carbon nanotubes produced onto iron catalysts [34–37,39]. In those studies, high conversions of 4-NP were achieved, but generally ascribed to an homogenous contribution, as consequence of iron leaching to the reaction media, which results in an additional contamination. In a previous work [40], reduced graphene oxides (a metal-free catalyst) were used in the CWPO of 4-NP, leading to maximum 4-NP conversions of 60% after 24 h under the following operating conditions: 50 °C, initial pH of 3 and concentration of 4-NP, H_2O_2 and catalyst of 5.0, 17.8 and 2.5 $g \cdot L^{-1}$, respectively.

Among the operating conditions of the CWPO process, the pH of the reaction medium can have a significant effect, depending on the pollutant and catalyst considered [34,36,41,42]. In CWPO kinetic studies, the pH effect is usually first studied in order to establish the adequate pH range for the catalytic performance and the kinetic model is later developed for that specific pH [43–45]. In this sense, it should be noted that reports dealing with kinetic studies and investigating the effect of the initial pH in CWPO do not consider the pH contribution in the developed kinetic model (even observing a significant effect of pH), neither the leached iron species nor the pH evolution of the medium with the reaction time [43–45]. In the few kinetic studies related to the peroxidation of 4-NP [35,46], the pH is never considered in the development of the kinetic model.

It has been observed, in the CWPO process of some pollutants, that the concentration evolution through the reaction time shows a transition regime between the initial slow degradation of the pollutant (induction period) and the subsequent rapid concentration decay (*S*-shaped curve) [34,36,47–51]. Some kinetic models are able to describe the *S*-shaped curves for the degradation of compounds that have been already reported in literature - as the autocatalytic model [52] or the empirical Fermi equation (mostly employed in literature to describe microbiological decays) [53]. Both of them have been employed or adapted to predict data in oxidation processes [47–51].

The current work deals with the development of a kinetic model for the CWPO of 4-NP, allowing the prediction of the effect of the aqueous solution pH evolution with reaction time. Non-porous metal-free carbon black (CB) is used as pristine material, since it was found to be an efficient and stable catalyst for CWPO [32] and since it is possible to increase its catalytic activity by proper doping with P, N and B, as previously demonstrated [33].

2. Materials and methods

2.1. Chemicals

CB was supplied in powder form by Chemviron (ref.:2156090). Boric acid (H_3BO_3, > 99.5 wt.%), pyridine (99.8% w/v) and urea (($NH_2)_2CO$, > 99 wt.%), used as precursors in the preparation of the doped catalysts, were supplied from Sigma-Aldrich. The other precursor used, phosphoric acid (H_3PO_4, 85% w/v), was purchased from Panreac. H_2O_2 solution (30% w/v), used as oxidant in the treatment of the synthetic wastewater, was purchased from Fluka. Titanium (IV) oxysulphate (TiOSO$_4$, 15 wt.% in dilute sulphuric acid, H_2SO_4 99.99%), hydrochloric acid (HCl, 37 wt.%) and sodium sulphite (Na$_2$SO$_3$, 98 wt.%) were purchased from Sigma-Aldrich. Sodium hydroxide (NaOH, 98 wt.%) was obtained from Panreac. 4-NP (98 wt.%) and 4-nitrocatechol (4-NC, 98 wt.%), acquired from Acros Organics and Fluka, respectively, were used to prepare working standard solutions for High Performance Liquid Chromatography (HPLC). Methanol (HPLC grade), glacial acetic acid (analytical reagent grade) and acetonitrile (HPLC grade) were obtained from Fisher Chemical. All chemicals were used as received without further purification. Distilled water was used throughout the work.

2.2. Preparation of doped carbon blacks

Doped CBs (DCBs) were prepared by a thermal-treatment carried out after the doping procedure under N_2 flow (50 Ncm^3 min^{-1}), from room temperature until 900 °C (considering a heating ramp of 10 °C·min^{-1}), during 24 h, as described elsewhere [33]. Briefly, P-DCB was prepared with H_3PO_4, which was heated up to the boiling temperature and fed into the oven, once the CB was loaded, by bubbling a N_2 stream used as saturated carrier gas. The precursors ($NH_2)_2CO$ or H_3BO_3 were physically mixed with CB powder and the resulting materials loaded into the oven in order to prepare N-DCB or B-DCB, respectively. In all cases, the precursor was used in excess assuring a molar ratio of element to CB equal to 5 (carbon content of the pristine CB is 98%). After the mentioned treatment, each sample was washed several times with deionized water until the pH of the rinsing waters was stabilized and further dried at 110 °C for 24 h.

2.3. Characterization techniques

The degree of wetting (wettability) of the DCBs (in the form of buckypapers) was determined by measuring the water contact-angle with an Attension Optical Tensiometer (model Theta) that allows the image acquisition and data analysis. The measurements with water were performed on dry buckypapers using the sessile-drop method. Each contact angle was measured at least in five different locations on the buckypapers to determine the average value. Buckypapers using different CB samples were obtained following a methodology adapted from elsewhere [39]. In a typical procedure, the CB material was dispersed in propan-2-ol (1 $g \cdot L^{-1}$) for 10 min by using an ultrasonic processor (UP400S, 24 kHz). Then, the CB suspension was filtered under vacuum through a polyethersulfone (PES) membrane (0.22 μm, Millipore) placed into a filtration device. Then, the formed buckypaper was taken off the PES membrane, placed between two cellulose discs and dried by a controlled heating until 100 °C in an oven.

The textural properties of the materials were determined from N_2 adsorption–desorption isotherms at 77 K, obtained in a Micromeritics Tristar 3000 apparatus. The BET surface area (S_{BET}) was calculated using the BET method, whereas the external surface area (S_{ext}) and micropore volume (V_{mic}) were obtained by the *t*-method (thickness was calculated by employing ASTM standard D-6556-01) [54]. The microporous surface area (S_{mic}) was determined as the subtraction of S_{ext} from S_{BET} ($S_{mic} = S_{BET} - S_{ext}$).

The size of the particles of CB and DCBs samples were analyzed in a laser diffraction equipment Malvern Mastersizer 3000, equipped with a dispersion unity Hydro MV (Malver, United Kingdom). Distilled water was used as solvent to disperse the materials and the analysis were made by using five measurements for each sample, which allowed to determine number distribution of the samples.

2.4. CWPO experiments

Batch CWPO experiments were carried out in a 250 mL well-stirred (600 rpm) glass reactor equipped with a condenser, a thermocouple, a pH measurement electrode and a sample collection port. A concentrated (5.0 $g \cdot L^{-1}$) 4-NP solution was considered as a model system to simulate high-loaded wastewaters [39]. The reactor was loaded with 50 mL of the 4-NP aqueous solution and heated by immersion in an oil bath at controlled temperature. Upon stabilization at the desired temperature, the solution pH was adjusted to a previously chosen value by means of H_2SO_4 and NaOH solutions, and the experiments were allowed to proceed freely, without further pH adjustment. Then, the adequate quantity of 30% w/v H_2O_2 (17.8 $g \cdot L^{-1}$) was added in order to use the stoichiometric dosage of H_2O_2 needed for complete 4-NP mineralization. Finally, the selected amount of catalyst was added, after complete homogenization of the resulting solution, that moment being considered as the initial reaction time, t_0 = 0 min.

Table 1
Relevant textural and chemical properties of the fresh CB and DCB catalysts.

Catalyst	S_{BET}, S_{ext} (m²/g)	P*, B* or N** (wt.%), [33]	Acidity (mmol·g⁻¹), [33]	pH_{PZC}, [33]	Contact angle	
					(°)	(photograph)
CB	73	P = 0.00 B = 0.00 N = 0.04	0.60	6.4	115 ± 1	
P-DCB	82	P = 0.04	1.33	3.5	39 ± 3	
B-DCB	84	B = 0.51	1.28	5.6	31 ± 2	
N-DCB	59	N = 0.37	0.55	6.0	121 ± 1	

* Phosphorous and Boron measured by ICP analysis.

** Nitrogen measured by elemental analysis (EA).

All runs were conducted during 24 h and considering a catalyst concentration of 2.5 g·L⁻¹. The temperature and initial pH of the reaction media were T = 50–80 °C and pH = 2–4. Blank experiments, in the absence of catalyst, were also carried out to observe the non-catalytic contribution to the pollutant degradation.

2.5. Analytical methods

Small aliquots were periodically withdrawn from the reactor to determine 4-NP, its oxidized intermediates and H_2O_2 concentration by HPLC and a colorimetric method, as previously described [34,38]. Briefly, 4-NP and its aromatic oxidation products (hydroquinone, 1,4-benzoquinone, 4-nitrocatechol, catechol and phenol), low molecular weight carboxylic acids (formic, acetic, oxalic, malonic, maleic and malic acids) and nitrates, were determined by using a Jasco HPLC system at wavelengths of 318, 277 and 210 nm (UV-2075 Plus detector), respectively. 4-NP and its aromatic intermediates were determined by using a Kromasil 100-5-C18 column and 1 mL·min⁻¹ (PU-2089 Plus) of an A:B (40:60) mixture of 3% acetic acid and 1% acetonitrile in methanol (A) and 3% acetic acid in ultrapure water (B). The low molecular weight carboxylic acids were monitored using an YMC–Triart C18 column and 0.6 mL·min⁻¹ of an A:B (95:5) mixture of 1% H_2SO_4 in ultrapure water (A) and acetonitrile (B). In order to determine the concentration of H_2O_2, a filtered sample was added to 1 mL of H_2SO_4 solution (0.5 mol·L⁻¹) in a 20 mL volumetric flask, to which 0.1 mL of $TiOSO_4$ were added. The resulting mixture was diluted with distilled water and further analyzed by UV–Vis spectrophotometry (T70 spectrometer, PG Instruments Ltd.)

2.6. Kinetic modelling

A kinetic study was done following the methodology considered in a previous work dealing with the CWPO of phenol at the initial pH of 3.5 (without variation of pH) [32,55,56]. The production rate, as r (mmol·h⁻¹·g⁻¹) of each given species i inside the batch-reactor was expressed considering a constant volume system, as shown in Eq. (1):

$$r_i = \frac{1}{W} \cdot \frac{dN_i}{dt} = \frac{1}{C_{cat}} \cdot \frac{dC_i}{dt} \tag{1}$$

where N_i and W are the moles of the compound i (mmol) and the catalyst mass (g) in the reactor, respectively, while C_i and C_{cat} are the corresponding concentrations, of that compound (mM) and the catalyst (g·L⁻¹); t is the time of reaction (h).

The numerical integration of the rate equations in a batch reactor with the initial conditions $C_i = C_{i,o}$ at $t = t_o$ was solved and the kinetic parameters were obtained by using the Microsoft Excel Solver (Microsoft Office 2013, MicrosoftCorp.) to minimize the sum of squared errors (SSE) of the relative concentration of i ($rc_i = C_i/C_{i,o}$) between the experimental (exp) and predicted (model) values (Eq. (2)):

$$SSE = \sum_{n=1}^{N} (rc_{exp\,i,n} - rc_{model\,i,n})^2 \tag{2}$$

rc was used to take into account the differences in the order of magnitude of the concentration among the compounds ($C_{4\text{-}NP}$ = 0–36 mM and $C_{H_2O_2}$ = 0 – 524 mM, whereas C/C_0 = 0–1 for each compound).

The models were also evaluated by the determination factor (R^2) calculated by applying Eq. (3), respectively:

$$R^2 = \frac{\sum_{n=1}^{N}(R.\,C_{\cdot model\,i,n} - R.\,C^-_{\cdot model\,i})^2}{\sum_{n=1}^{N}(R.\,C_{\cdot model\,i,n} - R.\,C^-_{\cdot modeli})^2 + \sum_{n=1}^{N}(R.\,C_{\cdot exp\,i,n} - R.\,C_{\cdot model\,i,n})^2} \tag{3}$$

where N is the total number of values (n) in a run and p is the number of predictors.

The equations were solved considering the Arrhenius equation (the influence of the temperature was considered directly in the model solution), thus calculating directly the activation energy and the pre-exponential factor.

3. Results and discussion

3.1. Characterization of the fresh DCBs

Table 1 summarizes BET and external surface area (S_{BET} and S_{ext}, respectively) and the most relevant properties of the pristine CB and DCB materials, reported in our previous work [33], such as content of heteroatoms, acidity and pH at the point of zero charge (pH_{PZC}). As

observed, values obtained of S_{BET} and S_{ext} were lower than 90 m^2 g^{-1}, which are low values of specific surface when compared to another carbonaceous materials [54] and consequently is not expected to observe a significant contribution in the removal of the pollutant by adsorption. In addition, the values of S_{BET} and S_{ext} were found to be close to each other, leading to a null micropore specific surface. According to the *t*-method, micropore volume is also null, consequently CB and P, N or B-DCB can be considered non-porous or macroporous materials. In fact, all isotherms adsorption of N$_2$ curves at 77 K (Fig. S1) can be classified as Type II isotherm that is typically given by the physisorption of most gases on nonporous or macroporous adsorbents. The shape is the result of unrestricted monolayer-multilayer adsorption up to high p/p^0. In addition, the absence of a hysteresis loop can be ascribed to the non-existence of narrow open ended pores.

The size of particles of the materials was found to present a narrow distribution from 45 to 990 nm (Fig. S2). The average particle size of the samples is 86 nm for the undoped material (CB) and 82, 89 and 90 nm for N-DCB, B-DCB and P-DCB, respectively. As observed, all materials present an average particle size close to the value found for the pristine material and the distribution of the particle size was also similar between them.

Additionally, Table 1 also shows the wettability of all materials as measured by the water contact-angle. As can be seen, the amount of doping element incorporated depends on the specific element, being higher for the DCB with boron and the doping method does not affect significantly the S_{BET} of the pristine material.

The P-DCB and B-DCB samples were found to present more acidity (1.28 and 1.33 mmol·g^{-1}, respectively), due to the presence of acid heteroatoms functional groups and surface carboxylic acid groups [33]. As a probable consequence, P-DCB and B-DCB are hydrophilic materials (as given by the low contact angles of 31 – 39°), meaning that increasing the acidity of CB, it is possible to increase its water-wettability. Additionally, the pH_{PZC} value of the P-DCB sample (3.5) suggest that the acidic groups in this material are stronger than in B-DCB [57,58]. The pristine material (CB) and the N-DCB show a low acidity (0.60-0.55 mmol·g^{-1}) and the highest values of the contact angle (115–121°).

A deeper discussion about the doping characterization of the DCBs can be found in the previous work [33].

3.2. Catalytic performance of DCBs in CWPO

The catalytic activity of the DCBs was assessed in the CWPO of 4-NP and compared to the non-catalytic wet peroxide oxidation (WPO) process. Pure adsorption contribution to the overall 4-NP uptake was not determined, since it was verified previously that it is negligible [32,33]. The evolution of 4-NP and H$_2$O$_2$ concentrations against reaction time were depicted in Fig. 1. The conversion of 4-NP (Fig. 1a) with the pristine material (CB) reached 6.8% after 24 h of time of reaction, which is similar than the conversion found in the non-catalytic run (5.8%). However, higher conversions of H$_2$O$_2$ (19.5%) were achieved with CB when compared to the non-catalytic run (< 7%). Thus, the consumption of H$_2$O$_2$ is not efficient when CB is used, evidencing the need to increase its catalytic activity in the oxidation of 4-NP. In this sense, the doping methods used to modify the commercial CB were found to lead successfully to an increment of the catalytic activity, since the conversion of 4-NP in the CWPO process was considerably higher with DCBs than with the undoped CB. More precisely, 4-NP conversions of 95.9, 65.5 and 40.4% were found after 24 h of reaction time with P-DCB, B-DCB and N-DCB, respectively. The highest catalytic activity exhibited by P-DCB and B-DCB can be ascribed to their chemical properties (Table 1). P-DCB and B-DCB are the catalysts tested with highest acidity (1.28 and 1.33 mmol·g^{-1}) and hydrophilic character (contact angles of 31 and 39°, respectively, Table 1), probably improving the reactants diffusion. An increment in the catalytic activity increasing the acidity of the catalyst was also observed in the CWPO of phenol [33]. The highest catalytic activity exhibited by P-DCB when
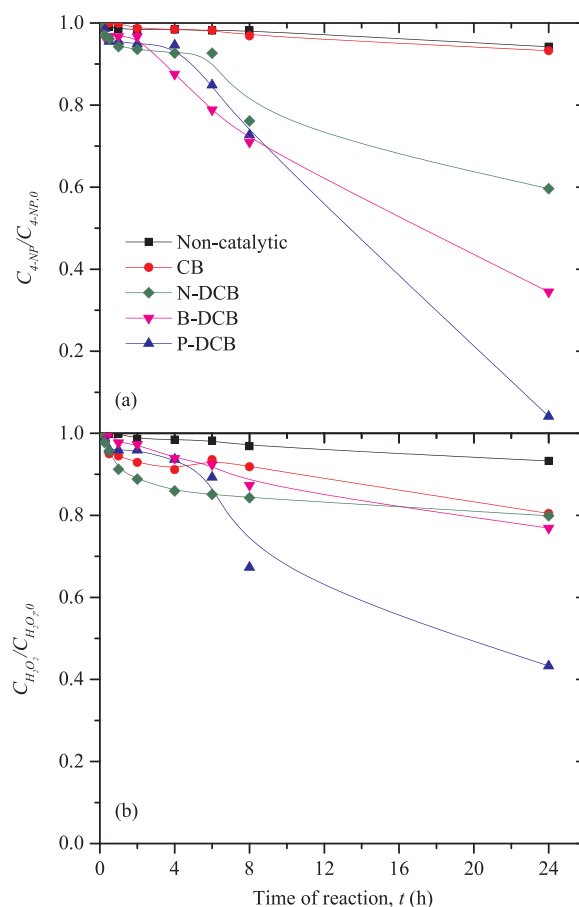

Fig. 1. Effect of carbon black doping on the evolution of the relative concentration of (a) 4-NP and (b) H$_2$O$_2$. Experimental conditions: C_{cat} = 2.5 g·L^{-1}, $C_{4\text{-}NP,0}$ = 5 g·L^{-1}, $C_{H_2O_2,0}$ = 17.8 g·L^{-1}, 50 °C and pH_0 3.

compared to B-DCB was ascribed to its lower pH_{PZC} value (Table 1). The strongest acidity of the P-DCB is consistent with other H$_3$PO$_4$-actived carbons, whereas the treatment with H$_3$BO$_3$ provokes an increase of the acidity in lower extent [33,59].

It should be noted that the conversion of 4-NP after 24 h is higher when compared to previous results (maximum conversion less than 70% after 24 h) obtained with metal-free graphene oxide catalysts under the same operating conditions [40]. However, when results are compared at low reaction times (< 2 h) with the previous study, the conversion of 4-NP achieved with P-DCB is lower, so the oxidation of 4-NP began to be significant only after 2 h. The consumption of H$_2$O$_2$ is also low at the initial stages of reaction and increase substantially after 2 h of reaction, revealing an induction period in the peroxide oxidation of 4-NP in the presence of the prepared carbon black catalysts. As can be observed, the induction period varied among the experiments performed with the different catalysts, ranging from 1 h (P-DCB) to 4 h (N-DCB). Interestingly, the occurrence of an induction period, from 10 min to 1 h, was also observed in the CWPO of 4-NP with Fe anchored catalysts [34,36]. To explain the presence of this induction period, Zhang et al. postulated [36] the formation of hydroperoxyl/superoxide radicals (HO$_2^{\bullet}$/O$_2^{\bullet-}$) on the surfaces sites of the solid catalyst. These reactive oxygen species HO$_2^{\bullet}$ and O$_2^{\bullet-}$ present a potential of oxidation, which is much lower than that of the HO$^{\bullet}$ species and, as consequence, a slow period of 4-NP removal appears initially.

In a previous work dealing with the CWPO of phenol with the DCB materials [33], an induction period was not detected. Therefore, the induction period has been found to be characteristic of the CWPO of 4-NP with DCB. During all experiments, 4-nitrocatechol (4-NC) was identified as oxidized intermediate of the 4-NP oxidation, but the
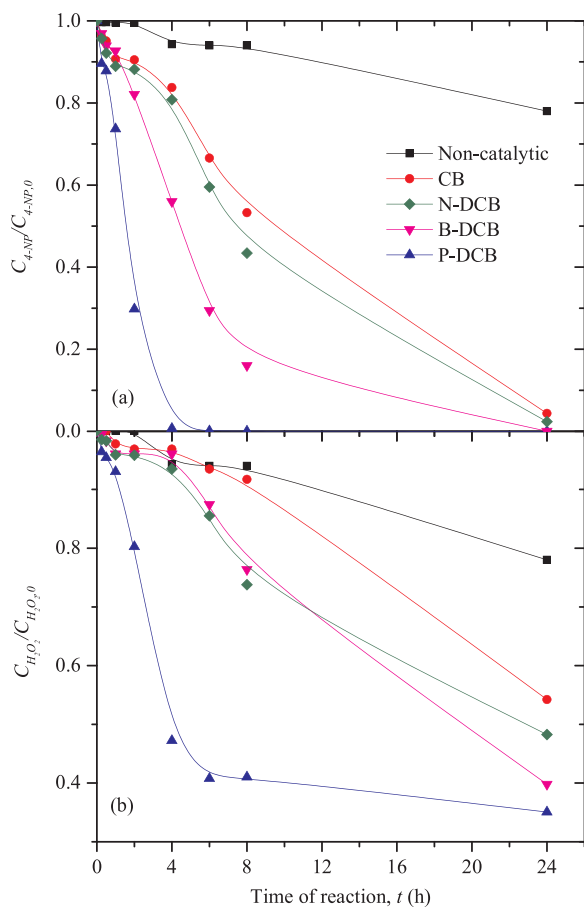
Fig. 2. Evolution of (a) 4-NP and (b) H_2O_2, as a function of reaction time with carbon blacks at 80 °C. Experimental conditions: $C_{cat} = 2.5$ g·L^{-1}, $C_{4-NP,0} = 5$ g·L^{-1}, $C_{H2O2,0} = 17.8$ g·L^{-1} and pH_0 3.

presence of 4-NC is only significant after the induction period. However, experiments carried out in the presence of 4-NC at the beginning of reaction evidenced that the oxidized intermediate does not work as redox initiator to promote the decomposition of H_2O_2 (Fig. S3). In this regard, it is also interesting to note that the CWPO run of 4-NC (without 4-NP) did not show any induction period with P-DCB.

3.3. Effect of temperature

Fig. 2 shows the relative concentration of 4-NP and H_2O_2 against the time of reaction with undoped CB, all DCBs and in the absence of catalyst at the higher tested temperature (80 °C). As observed, the removal of 4-NP without catalyst is significantly lower (21.9% after 24 h of reaction time) when compared to the catalytic runs (almost complete conversion of 4-NP after 24 h with the undoped material and P, B or N-DCB). The increment of reaction temperature contributes to enhance the 4-NP oxidation rate, due to a faster decomposition of H_2O_2, as observed in Fig. 2.b. Further analysis of Fig. 2 shows that the complete conversion of the pollutant is achieved with P-DCB after 4 h of reaction time, whereas 44%, 19.2% and 16.2% of 4-NP conversion is reached with B-DCB, NDCB and the pristine material, respectively. Same order of catalytic activity P-DCB > B-DCB > N-DCB > CB is found at 50 °C obtaining 4-NP conversions from 12% to 5% with DCB and 1.5% with the un-doped catalyst after 4 h (2.5–18 times higher 4-NP removals were obtained at 80 °C and 4 h of time of reaction). An induction period is also observed at 80 °C, but its duration is shorter than the induction period observed at 50 °C. This means that the effect of temperature in the CWPO of 4-NP is very significant in such a way that the increase of the temperature, not only increases the rate of peroxide oxidation, but

also reduces the induction period, allowing to achieve higher conversion values in lower reaction times. At 80 °C, the presence of 4-NC was also found to be significant only after the induction period.

3.4. Effect of pH

The influence of the initial pH (pH_0) was analysed in the range from 2 to 4 (not buffered), considering the CWPO of 4-NP with the most active catalyst, P-DCB, at 50 °C. In these experiments, the pH of the aqueous solution was followed during the time of reaction. The profiles of H_2O_2, 4-NP and 4-NC concentration are depicted in Fig. 3 against time of reaction (left) and pH (right). As it can be observed, the initial pH of the aqueous medium has a significant effect on the process, since the decrease of pH_0 leads to the increase of H_2O_2 (Fig. 3a) and 4-NP (Fig. 3c) conversions in the CWPO process with PDCB. In fact, a 4-NP conversion of 99.3% is achieved at pH_0 2 and 8 h of reaction, whereas 33.5% was found at pH_0 3. The curve of 4-NC concentration (Fig. 3e) shows a faster apparition and oxidation of this compound at pH_0 2 as compared to the behavior observed under a higher initial pH value in the CWPO process. Accordingly, the initial pH of the CWPO process of 4-NP with P-DCB can be adjusted for the benefit of the parent pollutant and intermediate conversion. The increment of the pollutant conversion can be ascribed to a higher rate consume of hydrogen peroxide, as can be observed in experiences of CWPO (Fig. 3a) and in runs of H_2O_2 decomposition carried out in absence of pollutant (Fig. S4). In consequence, it is hoped that rate production of hydroxyl and hydroperoxyl radical would be increased, leading an oxidation kinetic of the model pollutant higher.

As observed, the effect of pH on the conversion of 4-NP is more significant than in the consumption of H_2O_2, since the conversion of the pollutant is increased from 9.7% to 93.4% after 6 h of reaction when pH decreases from 4 to 2, respectively, whereas the consumption of H_2O_2 is only increased from 6.9% to 30.1%. This can be explained by the fact that the concentration of H_2O_2 was considered to be the stoichiometric amount needed to mineralize 4-NP, thus the consumption of H_2O_2 is not directly related to the conversion of 4-NP, but rather to the mineralization extent (not included in this work). Interestingly, most of the works in the literature studied how the pH affects the conversion of the model pollutant under study, but not the effect of the pH on the consumption of H_2O_2 [34,36,43,60]. A significant effect of the pH on the conversion of both pollutant and H_2O_2 has been found in the CWPO of phenol with Fe/γ-Al$_2$O$_3$ [41].

The effect was more significant in the removal of the pollutant than in the consumption of H_2O_2 as observed in this work. Another possible explanation may be related to an increase in the efficiency of H_2O_2 consumption (defined as ratio of TOC to H_2O_2 conversion) as pH decreases, as observed in the CWPO of phenol with gold/activated catalyst, decreasing the initial pH of reaction media from 10.5 to 3.5 [44]. That means that higher removals of organic compounds can be achieved by decreasing the pH without further non-efficient consumption of H_2O_2.

As expected, the pH of the aqueous system decreases with reaction time (Fig. 3 right), as a consequence of the acids generated from the peroxide oxidation of 4-NP [40]. The pH evolution in the experiences of CWPO of 4-NP can be ascribed to the denitrification of 4-NP and 4-NC, and to the production of ring opening species, which are mostly low molecular weight carboxylic acids. The low molecular weight acids identified in the CWPO of 4-NP with P-DCB by using HPLC were malic, maleic, malonic, oxalic, acetic formic and nitric acid (Fig. S5 shows the concentration of these compounds after 6 h of time of reaction at pH_0 2, 3 and 4). The pH curves show an inflection point at pH value around 2.5 from that value, where the reaction accelerates and a significant increment of the 4-NP and H_2O_2 conversions was observed. The turning point of pH 2.5 is reached between 2 and 4 h of reaction (times of reaction included in Fig. 3.b-d-f) at pH_0 3 and pH_0 4, respectively. Therefore, a decrease in the initial pH leads to a decreasing of the
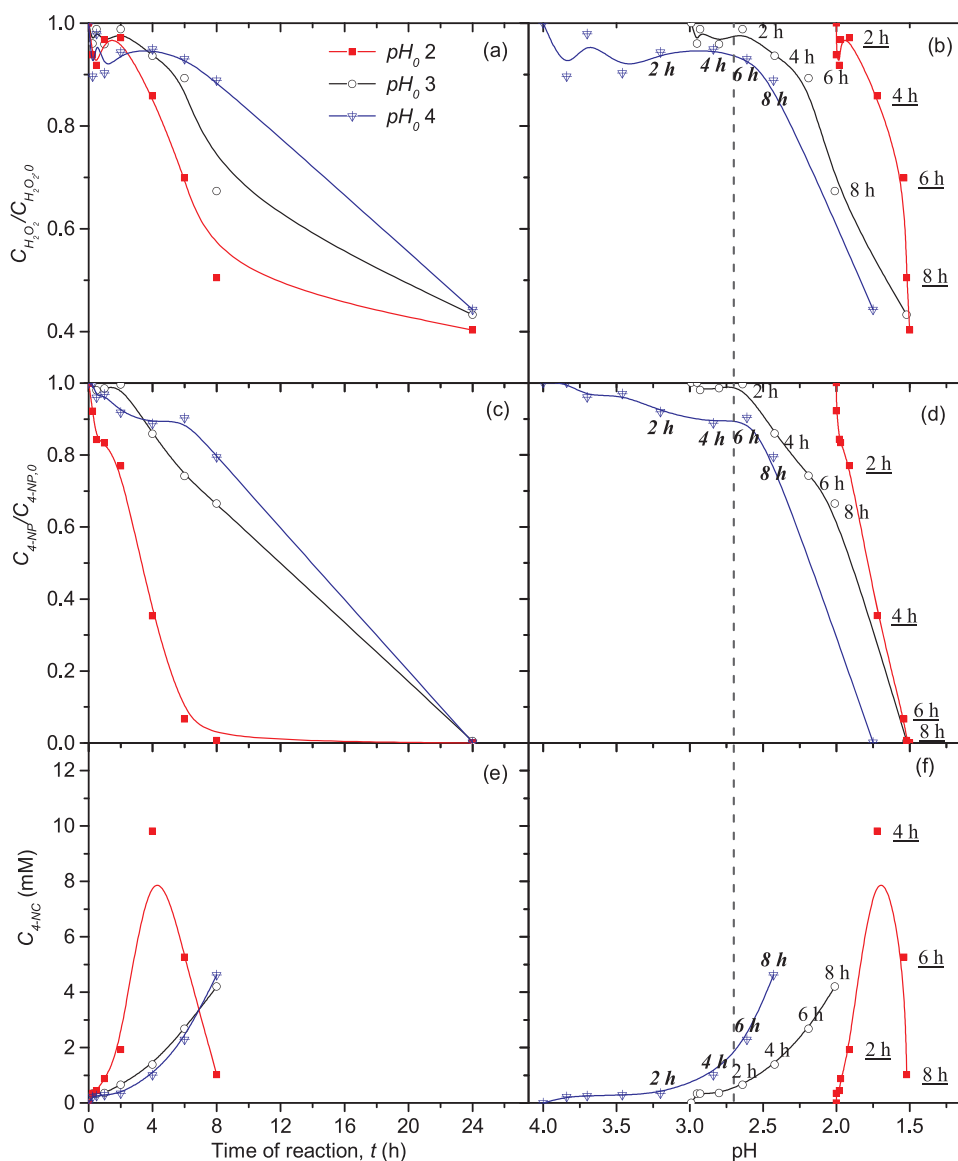
Fig. 3. Effect of the initial pH (pH_0) on the evolution of (a,b) H_2O_2, (c,d) 4-NP and (e,f) 4-NC, as a function of reaction time (left) and the pH of the reaction medium (right). Inserted numbers (b, d, f) represent the reaction time in hours. Experimental conditions: $C_{P\text{-}DCB} = 2.5$ g·L^{-1}, $C_{4\text{-}NP,0} = 5$ g·L^{-1}, $C_{H2O2,0} = 17.8$ g·L^{-1} and 50 °C.

induction period, which is negligible at pH_0 2.

3.5. Kinetic modelling

Kinetic modelling was performed taking into account the absence of transfer limitations at the operating conditions tested, since the catalyst was used in powder form (average particle size of 89 nm) and the appropriate stirring velocity were used (stirring velocity was not found to affect the conversion of 4-NP, TOC and H_2O_2). In addition, the adsorption contribution in the removal of pollutants with these non-microporous materials is negligible. Therefore, it is not expected that kinetic will be limited by internal diffusion limitations, since non-porous material with small particle size (Fig. S2) is used.

Three kinetic models with different equations, summarized in Table 2, were tested for all permutations of kinetic order (from 0 to 2). The homogeneous non-catalytic contribution was not considered due to the low 4-NP conversions obtained at 50 and 80 °C without catalyst (Figs. 1 and 2, respectively). All kinetic models were developed taking into account the pH of the reaction media, which was included assuming the appearance rate of any compound (i) directly proportional to the concentration of protons (Eq. (4)):

$$C_{H^+} = 10^{-pH} \tag{4}$$

The concentration of the protons in the solution depend on the acid dissociation constant (K_a) of all carboxylic and nitric acids produced, and how the dissociation is affected by the presence of each of them. This means that the protons concentration is a complex function that depends on the concentrations of all substances present in the matrix and their properties. Including the protons concentration in the appearance rate is just like modelling the lumped acids. Taking into account previous reports [32,40], as well as the above discussion about the reaction intermediates resulting from the oxidation of 4-NP (4-NC and carboxylic and nitric acids), a generalized reaction pathway is proposed (Fig. 4), where the assumption of the lumped acids is placed in evidence. The pH evolution in the experiments of CWPO of 4-NP, ascribed to the denitrification of 4-NP and 4-NC, and ring opening products, has to be necessarily modelled in order to predict the 4-NP oxidation and H_2O_2 consumption rates with accuracy. The pH results were taken into account, specially interesting in the process, since the pH_0 affects strongly the induction period and the oxidation rate of 4-NP.

Regarding H_2O_2, it is known that its decomposition yields hydroxyl and hydroperoxy radicals at the carbon surface sites (SS) and these

Table 2

Proposed kinetic models used to fit the rate of consumption and formation of the compounds 4-NP, H_2O_2 and H^+ in the CWPO of 4-NP with P-DCB.

Kinetic model I

$$-\frac{dC_{4-NP}}{dt} = k_{4-NP}\cdot C_{4-NP}{}^{n_{4-NP}^I}\cdot C_{H_2O_2}{}^{n_{H_2O_2}^I}\cdot C_{H^+}{}^{n_{H^+}^I}$$

$$-\frac{dC_{H_2O_2}}{dt} = k_{H_2O_2}\cdot C_{4-NP}{}^{n_{4-NP}^{II}}\cdot C_{H_2O_2}{}^{n_{H_2O_2}^{II}}\cdot C_{H^+}{}^{n_{H^+}^{II}}$$

$$\frac{dC_{H^+}}{dt} = k_{H_2O_2}\cdot C_{4-NP}{}^{n_{4-NP}^{III}}\cdot C_{H_2O_2}{}^{n_{H_2O_2}^{III}}\cdot C_{H^+}{}^{n_{H^+}^{III}}$$

Kinetic model II

Modelling one of the main compounds (i = 4-NP, H_2O_2, or H^+) with Fermi equation:

$$-\frac{dC_i}{dt} = k_i\cdot C_i{}^{n_i^I}\cdot C_j{}^{n_j^I}\cdot C_m{}^{n_m^I}\cdot\frac{\exp(k\cdot(t-t^*))}{1+\exp(k\cdot(t-t^*))}$$

and the rest of them by power-law potential model (j and $m \neq i$):

$$-\frac{dC_j}{dt} = k_j\cdot C_i{}^{n_i^{II}}\cdot C_j{}^{n_j^{II}}\cdot C_m{}^{n_m^{II}}$$

$$-\frac{dC_m}{dt} = k_m\cdot C_i{}^{n_i^{III}}\cdot C_j{}^{n_j^{III}}\cdot C_m{}^{n_m^{III}}$$

That results in 3 systems of equations (one for each Fermi equation used in the disappearance rate of one of the three main compounds: 4-NP, H_2O_2, and H^+).

Kinetic model III

Modelling one of the main compounds (i = 4-NP, H_2O_2, or H^+) by using autocatalytic model:

$$-\frac{dC_i}{dt} = k_i\cdot C_i{}^{n_i}\cdot(C_0 - C_i)\cdot C_j{}^{n_j}\cdot C_m{}^{n_m}$$

and the rest of them by power-law potential model (j and $m \neq i$):

$$-\frac{dC_j}{dt} = k_j\cdot C_i{}^{n_i^{II}}\cdot C_j{}^{n_j^{II}}\cdot C_m{}^{n_m^{II}}$$

$$-\frac{dC_m}{dt} = k_m\cdot C_i{}^{n_i^{III}}\cdot C_j{}^{n_j^{III}}\cdot C_m{}^{n_m^{III}}$$

That results in 3 systems of equations (one for each autocatalytic model used in the disappearance rate of one of the three main compounds: 4-NP, H_2O_2, and H^+).

---

radicals further react with the organic matter in the liquid phase [32]. Thus, H_2O_2 disappearance can be described by the reaction:

$$SS + 2\ H_2O_{2aq} \rightarrow 2\ SS(H_2O_2)_s \rightarrow HO^\bullet + HOO^\bullet + OH^- + H^+$$
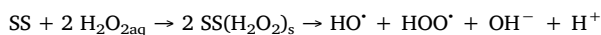
Oxidation of 4-NP to 4-NC, its denitrification to phenol and/or hydroquinone (which could be produced from phenol) may be considered. 4-NC may be denitrified to catechol or, as many other aromatic compounds produced, oxidized to ring opening products.

The induction period has to be considered using the kinetic models able to describe the *S*-shaped curves reported in the introduction (autocatalytic model [52] and Fermi equation [53]). The autocatalytic system and the Fermi equation are typically represented as Eqs. (5) and (6), respectively:

$$\frac{dC_i}{dt} = k\cdot C_i\cdot(c_0 - C_i) \tag{5}$$

$$C_i = \frac{C_{i,0}}{1 + \exp(k\cdot(t - t^*))} \tag{6}$$

where C_O and t^* are constants to fit. Theoretically, C_O represents the sum of the concentration of a reagent (C_i) and a product (C_R), which in turn works as reagent, also reacting with a molar ratio 1:1 with the reagent i ($i + R \rightarrow R + R$), resulting in a constant concentration ($C_O = C_{i,0} + C_{R,0} = C_i + C_R$). This means that increasing the content of the product (R), the rate is increased, since the own product play a role as reagent. For this reason, the model can be used to represent *S*-shape curve profile. For its part, the t^* constant in the Fermi equation corresponds to the time of the inflexion point in the *S*-shaped curve profiles. From the Fermi equation (Eq. (6)), the disappearance rate of a compound i can be developed by the analytical integration, as given by Eq. (7):

$$\frac{dC}{dt} = -k\cdot C\cdot\frac{\exp(k\cdot(t - t^*))}{1 + \exp(k\cdot(t - t^*))} \tag{7}$$

Then, the disappearance or appearance rate of each compound (4-NP, H_2O_2 and H^+) was modelled considering the concentration of each of them with different kinetic orders and the power-law potential, Fermi equation and autocatalytic model for each of them too.

The kinetic order of the compounds 4-NP and H_2O_2 were permuted to be integer numbers, whereas the kinetic order of protons concentrations was optimized in the range 0–2 to take any value. The kinetic model including the autocatalytic equation to predict the H_2O_2 decomposition was found to simulate most suitably the CWPO of 4-NP, whereas the rest of species (4-NP and H^+) are best modelled by using a kinetic potential equation. As concentration of protons increased during the reaction time, the inverse relative concentration was considered to
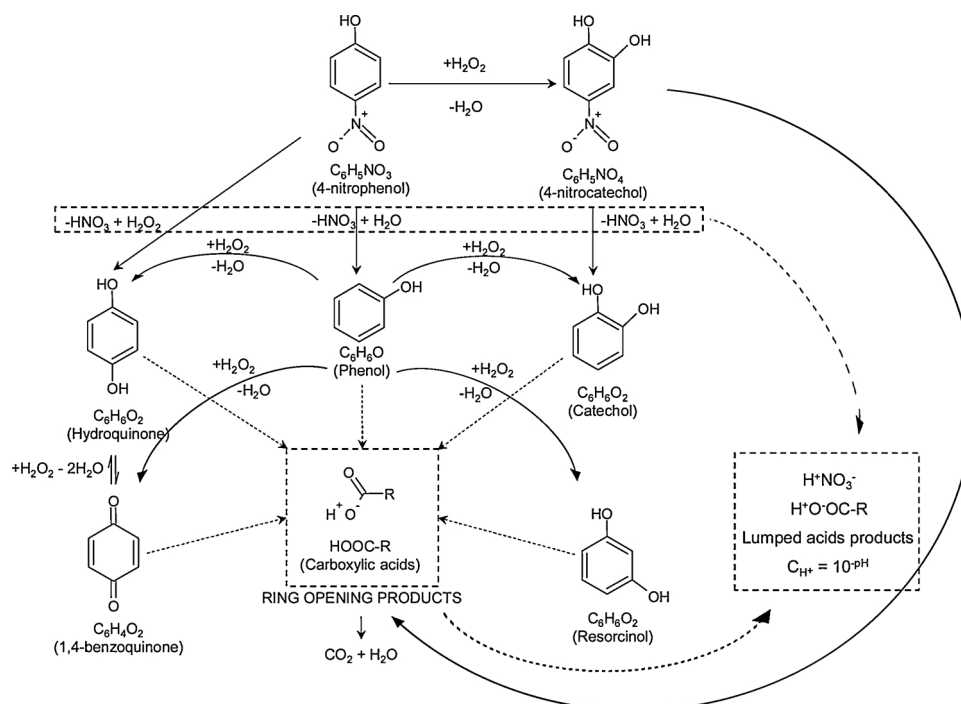

Fig. 4. Reaction pathway of the CWPO of 4-NP using P-doped carbon black as catalyst.

Table 3

Kinetic model of 4-NP based on autocatalytic reaction mechanism for the decomposition of H_2O_2 in the CWPO with P-DCB as catalyst (units in mM and min).

Kinetic equation	R^2	SSE
$\frac{dC_{4\text{-}NP}}{dt} = -3.6\cdot10^{10}\cdot exp\left(\frac{-102\,kJ/mol}{R\cdot T}\right)\cdot C_{4\text{-}NP}\cdot C_{H_2O_2}\cdot C_{H^+}$	0.96	0.19
$\frac{dC_{H_2O_2}}{dt} = -7.2\cdot10^{9}\cdot exp\left(\frac{-103\,kJ/mol}{R\cdot T}\right)\cdot C_{4\text{-}NP}\cdot C_{H_2O_2}\cdot(524\,mM - C_{H_2O_2})\cdot C_{H^+}$	0.91	0.83
$\frac{dC_{H^+}}{dt} = 5.1\cdot10^{-3}\cdot C_{H^+}^{0,77}$	0.98	1.09

minimize the *SSE* to take into account the differences in the order of magnitude of the concentration among the compounds. Then, the fitting of the model to the experimental data through to minimize *SSE* of the model as an objective function with the same weight for the SSE of each relative concentration as follow (Eqs. (8)–(11)):

$$SSE_{4\text{-}NP} = \sum_{n=1}^{N}\left(\frac{C_{4\text{-}NP}}{C_{4\text{-}NP,0}}_{exp\,i,n} - \frac{C_{4\text{-}NP}}{C_{4\text{-}NP,0}}_{model\,i,n}\right)^2 \quad (8)$$

$$SSE_{H_2O_2} = \sum_{n=1}^{N}\left(\frac{C_{H_2O_2}}{C_{H_2O_2,0}}_{exp\,i,n} - \frac{C_{H_2O_2}}{C_{H_2O_2,0}}_{model\,i,n}\right)^2 \quad (9)$$

$$SSE_{H^+} = \sum_{n=1}^{N}\left(\frac{C_{H^+,0}}{C_{H^+}}_{exp\,i,n} - \frac{C_{H^+,0}}{C_{H^+}}_{model\,i,n}\right)^2 \quad (10)$$

$$SSE = SSE_{4\text{-}NP} + SSE_{H_2O_2} + SSE_{H^+} \quad (11)$$

The estimated values of apparent activation energy (*Ea*), pre-exponential factor (k_0) and determination coefficient (R^2) are provided in Table 3. Concretely, the values of the kinetic constant obtained at 80 °C are: $k_{4\text{-}NP} = 2.2\cdot10^{-5}\,M^{-2}\,min^{-1}$, $k_{H_2O_2} = 4.0\cdot10^{-6}\,M^{-3}\cdot min^{-1}$ and $k_{H^+} = 5.1\cdot10^{-3}\,M^{-0.23}\,min^{-1}$ at 80 °C. The validation of this model was supported by the values of determination coefficients of the fitting and illustrated by the parity plots of Fig. 5 and from the analysis of variance of the model, since a F-value of Fischer of 68 was determined (higher than the *p-value* 2.1). The predicted evolution of the compounds (curves) with their experimental data (symbols) are depicted in Fig. 6.

According to this model, the evolution rate of 4-NP oxidation and H_2O_2 consumption were found to be dependent on the concentration of the compounds 4-NP, H_2O_2 and pH, as if the reaction order with respect to the reactants and the pH would be 1 ($n_{4\text{-}NP} = n_{H_2O_2} = n_{H^+} = 1$). The protons concentration was crucial in order to predict reasonably well the disappearance rate of the reagents. The slow initial rates of 4-NP

oxidation and H_2O_2 consumption, as consequence of the induction period, were suitably reproduced by the autocatalytic equation used to reproduce the concentration of H_2O_2 upon reaction time. Interestingly, the concentration of 4-NP was found to be indispensable to reproduce the asymptotic trend of the H_2O_2 concentration at high values of reaction time. That likely means that most of the compounds produced from the oxidation of 4-NP may be refractory while 4-NP is consumed.

It may be emphasized that the parameter C_0 of the autocatalytic kinetic equation, which is used to describe the evolution of H_2O_2, does not take similar values when it was used in the rate of the other compounds. Thus, it has not been possible to establish a theoretical relationship between compounds with C_0 in the way: $C_0 = C_{H_2O_2} + C_i$. We speculate that the modification of the catalyst during the reaction may be taking place, in such a way that its catalytic activity could be increased upon reaction time and, in consequence, acting as a trigger at specified time or pH. However, the second use of the catalyst shows a decrease of its catalytic activity in the CWPO of 4-NP.

Accordingly with the resultant model, the appearance rate of protons can be only predicted with its own concentration. However, the protons concentration depend on the concentration of the matrix compounds, including 4-NP and H_2O_2. The integer value for the reaction order of protons could not be a suitable choice to predict its experimental values (Fig. S6). The consideration of the pH value of the reaction medium to model the chemical kinetic oxidation of a target pollutant with H_2O_2 results a useful tool to take into account in future works of CWPO or AOPs. Integrate the pH value in a kinetic model allows not only the good simulation of the compounds removal in the oxidation process, but also the prediction of the pH evolution of the medium of reaction. This means that it is possible to select the most appropriate operating conditions to avoid the acid corrosion in a chemical reactor and the process lines or adjust the pH of the effluent when its value is a key output variable of design.

4. Conclusions

The catalytic activity of a commercial carbon black in the CWPO of 4-NP is increased by doping with P, B or N elements. Doping the carbon material with P led to obtain the most active catalyst in the process, as consequence of its strongest acidic nature and wetting degree. By increasing the temperature or the acidity of the reaction media it is possible to increase the conversion of the pollutant, since the oxidation rate is increased and the observed induction period decreased. The CWPO of 4-NP with the P-doped carbon black can be well-described by applying an empirical kinetic model composed by an autocatalytic expression, to describe the decomposition of H_2O_2, and by a power-law expression, to account for the evolution of 4-NP and H^+ (determined as $C_{H^+} = 10^{-pH}$). In this sense, it is possible to predict the induction period, which takes place in the process, and the evolution of the pH.
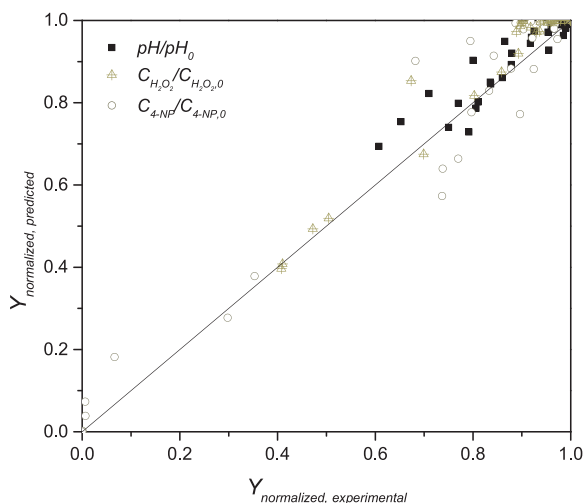
Fig. 5. Parity plots of normalized concentrations obtained by employing the resultant kinetic model (Table 3).
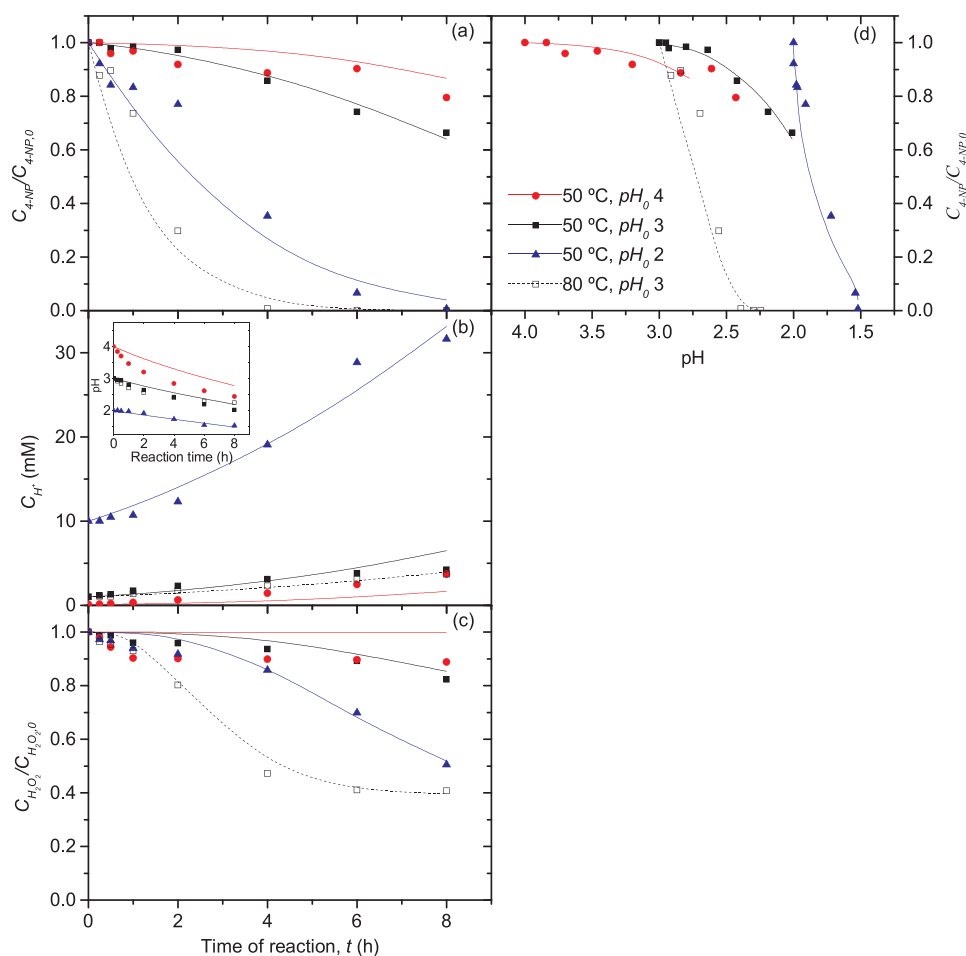
Fig. 6. Evolution of (a) 4-NP, (b) protons (Inset: as pH) and (c) H_2O_2 as a function of time; and the evolution of (d) 4-NP as a function of pH. Symbols as experimental data and curves as predicted values from the model. Experimental conditions: $C_{cat} = 2.5 \text{ g·L}^{-1}$, $C_{4\text{-}NP,0} = 5 \text{ g·L}^{-1}$ and $C_{H2O2,0} = 17.8 \text{ g·L}^{-1}$.

Appendix A. Supplementary data

Supplementary material related to this article can be found, in the online version, at doi:https://doi.org/10.1016/j.cattod.2019.08.033.

References

[1] F. Orshansky, N. Narkis, Water Res. 31 (1997) 391–398.
[2] A. Li, Q. Zhang, G. Zhang, J. Chen, Z. Fei, F. Liu, Chemosphere 47 (2002) 981–989.
[3] V. Kavitha, K. Palanivelu, J. Photochem. Photobiol. A Chem. 170 (2005) 83–95.
[4] M. Trapido, Y. Veressinina, J. Kallas, Ozone Sci. Eng. 23 (2001) 333–342.
[5] L. Keith, W. Telliard, Environ. Sci. Technol. 13 (1979) 416–423.
[6] Environmental Protection Agency, Nitrophenols, Ambient Water Quality Criteria, (1980), pp. A1–C134.
[7] F.E. Hancock, Catal. Today 53 (1999) 3–9.
[8] M. Munoz, F.J. Mora, Z.M. de Pedro, S. Alvarez-Torrellas, J.A. Casas, J.J. Rodriguez, J. Hazard. Mater. 331 (2017) 45–54.
[9] S. Azabou, W. Najjar, A. Bouaziz, A. Ghorbel, S. Sayadi, J. Hazard. Mater. 183 (2010) 62–69.
[10] R. Andreozzi, Catal. Today 53 (1999) 51–59.
[11] M. Hartmann, S. Kullmann, H. Keller, J. Mater. Chem. 20 (2010) 9002.
[12] O. Legrini, E. Oliveros, A.M. Braun, Chem. Rev. 93 (1993) 671–698.
[13] P.R. Gogate, A.B. Pandit, Adv. Environ. Res. 8 (2004) 501–551.
[14] S. Navalon, M. Alvaro, H. Garcia, Appl. Catal. B 99 (2010) 1–26.
[15] L. Gu, X. Zhang, L. Lei, Y. Zhang, Microporous Mesoporous Mater. 119 (2009) 237–244.
[16] C. Chen, H. Chen, J. Yu, C. Han, G. Yan, S. Guo, CLEAN Soil Air Water 43 (2015) 1010–1017.
[17] G. Mele, R. Del Sole, G. Vasapollo, E. García-López, L. Palmisano, M. Schiavello, J. Catal. 217 (2003) 334–342.
[18] R. Andreozzi, V. Caprio, A. Insola, G. Longo, V. Tufano, J. Chem. Technol. Biotechnol. 75 (2000) 131–136.
[19] Q. Dai, L. Lei, X. Zhang, Sep. Purif. Technol. 61 (2008) 123–129.
[20] Y. Jiang, Z. Hu, M. Zhou, L. Zhou, B. Xi, Sep. Purif. Technol. 128 (2014) 67–71.
[21] M. Trapido, J. Kallas, Environ. Technol. 21 (2010) 799–808.
[22] S. Barreca, J.J.V. Colmenares, A. Pace, S. Orecchio, C. Pulgarin, J. Photochem. Photobiol. A Chem. 282 (2014) 33–40.
[23] A. Goi, M. Trapido, Chemosphere 46 (2002) 913–922.
[24] J.A. Herrera-Melian, A.J. Martin-Rodriguez, A. Ortega-Mendez, J. Arana, J.M. Dona-Rodriguez, J. Perez-Pena, J. Environ. Manage. 105 (2012) 53–60.
[25] N. Wang, T. Zheng, J. Jiang, W.-s. Lung, X. Miao, P. Wang, Chem. Eng. J. 239 (2014) 351–359.
[26] Y.Y. Chu, Y. Qian, W.J. Wang, X.L. Deng, J. Hazard. Mater. 199-200 (2012) 179–185.
[27] H. Zhang, C. Fei, D. Zhang, F. Tang, J. Hazard. Mater. 145 (2007) 227–232.
[28] S. Yuan, M. Tian, Y. Cui, L. Lin, X. Lu, J. Hazard. Mater. 137 (2006) 573–580.
[29] Y.-S. Ma, S.-T. Huang, J.-G. Lin, Water Sci. Technol. 42 (2000) 1155–1160.
[30] J.J. Pignatello, E. Oliveros, A. MacKay, Crit. Rev. Environ. Sci. Technol. 36 (2006) 1–84.
[31] M. Pera-Titus, V. García-Molina, M.A. Baños, J. Giménez, S. Esplugas, Appl. Catal. B 47 (2004) 219–256.
[32] J.L. Diaz de Tuesta, A. Quintanilla, J.A. Casas, J.J. Rodriguez, Appl. Catal. B 209 (2017) 701–710.
[33] J.L. Diaz de Tuesta, A. Quintanilla, J.A. Casas, J.J. Rodriguez, Catal. Commun. 102 (2017) 131–135.
[34] R.S. Ribeiro, A.M.T. Silva, P.B. Tavares, J.L. Figueiredo, J.L. Faria, H.T. Gomes, Catal. Today 280 (2017) 184–191.
[35] S.-P. Sun, A.T. Lemley, J. Mol. Catal. A Chem. 349 (2011) 71–79.
[36] A. Zhang, N. Wang, J. Zhou, P. Jiang, G. Liu, J. Hazard. Mater. 201-202 (2012) 68–73.

[37] J. Yan, H. Tang, Z. Lin, M.N. Anjum, L. Zhu, Chemosphere 87 (2012) 111–117.
[38] M.S. Kalmakhanova, J.L. Diaz de Tuesta, B.K. Massalimova, H.T. Gomes, Environ. Eng. Res. 25 (2019) 186–196.
[39] M. Martin-Martínez, R.S. Ribeiro, B.F. Machado, P. Serp, S. Morales-Torres, A.M.T. Silva, J.L. Figueiredo, J.L. Faria, H.T. Gomes, ChemCatChem 8 (2016) 2068–2078.
[40] R.S. Ribeiro, A.M.T. Silva, L.M. Pastrana-Martínez, J.L. Figueiredo, J.L. Faria, H.T. Gomes, Catal. Today 249 (2015) 204–212.
[41] P. Bautista, A.F. Mohedano, J.A. Casas, J.A. Zazo, J.J. Rodriguez, J. Chem. Technol. Biotechnol. 86 (2011) 497–504.
[42] K. Fajerwerg, H. Debellefontaine, Appl. Catal. B 10 (1996) L229–L235.
[43] J. Guo, M. Al-Dahhan, Ind. Eng. Chem. Res. 42 (2003) 2450–2460.
[44] C.M. Domínguez, A. Quintanilla, J.A. Casas, J.J. Rodriguez, Chem. Eng. J. 253 (2014) 486–492.
[45] L. Xu, J. Wang, Environ. Sci. Technol. 46 (2012) 10145–10153.
[46] S. Minz, S. Garg, R. Gupta, Chem. Eng. Commun. 205 (2018) 667–679.
[47] A. Pintar, J. Levec, J. Catal. 135 (1992) 345–357.
[48] F. Arena, C. Italiano, A. Raneri, C. Saja, Appl. Catal. B 99 (2010) 321–328.
[49] A.M.T. Silva, J. Herney-Ramirez, U. Söylemez, L.M. Madeira, Appl. Catal. B 121-122 (2012) 10–19.
[50] J. Herney-Ramirez, A.M.T. Silva, M.A. Vicente, C.A. Costa, L.M. Madeira, Appl. Catal. B 101 (2011) 197–205.
[51] M. Bayat, M. Sohrabi, S.J. Royaee, J. Ind. Eng. Chem. 18 (2012) 957–962.
[52] O. Levenspiel, Chemical Reaction Engineering, 3rd edition, (1998).
[53] M. Peleg, J. Sci. Food Agric. 71 (1996) 225–230.
[54] J.L. Diaz de Tuesta, A.M.T. Silva, J.L. Faria, H.T. Gomes, Chem. Eng. J. 347 (2018) 963–971.
[55] A. Quintanilla, J.L. Diaz de Tuesta, C. Figueruelo, M. Munoz, J.A. Casas, Catalysts 9 (2019) 516.
[56] A. Quintanilla, J.L. Diaz de Tuesta, C. Figueruelo, M. Munoz, J.A. Casas, Catalysts 9 (2019) 518.
[57] B.L. Devi, K.N. Gangadhar, P.S. Prasad, B. Jagannadh, R.B. Prasad, ChemSusChem 2 (2009) 617–620.
[58] R.S. Ribeiro, A.M.T. Silva, J.L. Figueiredo, J.L. Faria, H.T. Gomes, Appl. Catal. B 140-141 (2013) 356–362.
[59] J. Bedia, J.M. Rosas, J. Márquez, J. Rodríguez-Mirasol, T. Cordero, Carbon 47 (2009) 286–294.
[60] N. Inchaurrondo, E. Contreras, P. Haure, Chem. Eng. J. 251 (2014) 146–157.